Non-Abelian Hyperbolic Band Theory from Supercells

Patrick M. Lenggenhager[1,2,3,4,*] Joseph Maciejko[4,5,†] and Tomáš Bzdušek[1,2,‡]

[1]*Department of Physics, University of Zurich, Winterthurerstrasse 190, 8057 Zurich, Switzerland*
[2]*Condensed Matter Theory Group, Paul Scherrer Institute, 5232 Villigen PSI, Switzerland*
[3]*Institute for Theoretical Physics, ETH Zurich, 8093 Zurich, Switzerland*
[4]*Theoretical Physics Institute, University of Alberta, Edmonton, Alberta T6G 2E1, Canada*
[5]*Department of Physics, University of Alberta, Edmonton, Alberta T6G 2E1, Canada*

Wave functions on periodic lattices are commonly described by Bloch band theory. Besides Abelian Bloch states labeled by a momentum vector, hyperbolic lattices support non-Abelian Bloch states that have so far eluded analytical treatments. By adapting the solid-state-physics notions of supercells and zone folding, we devise a method for the systematic construction of non-Abelian Bloch states. The method applies Abelian band theory to sequences of supercells, recursively built as symmetric aggregates of smaller cells, and enables a rapidly convergent computation of bulk spectra and eigenstates for both gapless and gapped tight-binding models. Our supercell method provides an efficient means of approximating the thermodynamic limit and marks a pivotal step toward a complete band-theoretic characterization of hyperbolic lattices.

Introduction.—Hyperbolic lattices are uniform discretizations of the two-dimensional (2D) hyperbolic plane with constant negative curvature. Recent experimental realizations in metamaterials, including coplanar-waveguide resonator [1] and electric-circuit networks [2], have elevated them from objects of academic interest to building blocks for engineering metamaterials. These advances have sparked a renewed interest in condensed-matter models on hyperbolic lattices, both in theory [3–20] and experiment [21–25]. The fundamental construction involves regular tessellations, where q copies of regular p-gons meet at each vertex, denoted by $\{p, q\}$ in Schläfli notation, with $(p - 2)(q - 2) > 4$.

For Euclidean lattices, Bloch's theorem labels Hamiltonian eigenstates by irreducible representations (IRs) of the translation group and enables a description in terms of a unit cell together with reciprocal space. While Bloch's theorem has been generalized [26–33] to hyperbolic lattices, this comes with fundamental difficulties. First, Bloch's theorem requires periodic boundary conditions (PBC), but constructing finite PBC clusters that approximate the thermodynamic limit is highly nontrivial [27,34,35]. Second, Euclidean translation groups are Abelian, such that only 1D IRs exist. In contrast, hyperbolic translation groups admit higher-dimensional IRs; therefore, hyperbolic band theory (HBT) requires non-Abelian Bloch states besides the usual Abelian ones [27]. We here refer to the approximation that considers only 1D IRs as Abelian HBT (AHBT) [26].

To deal with these difficulties, various avenues have been explored. Finite flakes with open boundary conditions exhibit a macroscopic fraction of boundary sites, which is advantageous when interested in boundary effects [10,15–17], but challenging when studying bulk properties. Good agreement of AHBT with bulk-projected spectra on flakes is observed in some models [10–12], but crucial features are missed in others [36]. Very recently, Lux and Prodan [34,35] have shown how to choose increasingly large PBC clusters to achieve convergence to the thermodynamic limit, while Mosseri and Vidal [37] have computed the density of states (DOS) of gapless models using a continued-fraction method. However, neither provides a reciprocal-space description, i.e., a description in terms of bulk states of the infinite lattice labeled by translation quantum numbers.

In this Letter, we introduce the supercell method to gain systematic access to non-Abelian Bloch states using AHBT combined with particular sequences of PBC clusters. We construct such sequences for various hyperbolic $\{p, q\}$ lattices using results from geometric group theory [38]. We observe rapid convergence of the DOS to the thermodynamic limit for various models. Our approach is computationally more efficient than real-space methods and affords the conceptual advantages of labeling eigenstates by momenta. We implement our algorithms in an open-source software package [39] for the computational algebra system GAP [40].

Supercells.—A lattice consists of copies of some chosen unit cell, generated by discrete translations forming a translation group Γ. While one commonly chooses a smallest primitive cell, implying a maximal translation group $\Gamma^{(1)}$, one can instead consider a supercell, i.e.,
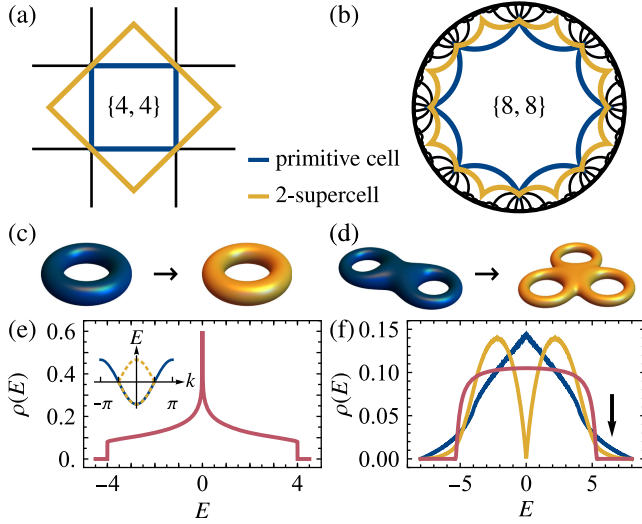
FIG. 1. Supercell construction for (a),(c),(e) the Euclidean $\{4,4\}$ and (b),(d),(f) hyperbolic $\{8,8\}$ lattice. (a),(b) Primitive cell (blue) and symmetrized 2-supercell (yellow). (c),(d) Compactified cells in real space. (e) Density of states ρ of the nearest-neighbor hopping model on the $\{4,4\}$ lattice as a function of energy E showing the characteristic van Hove singularity. The inset shows the momentum-space dispersion for the primitive cell (solid blue line) and for the supercell (yellow dashed line). (f) Density of Abelian Bloch states of the nearest-neighbor hopping model on the $\{8,8\}$ lattice for the primitive cell (blue), for the 2-supercell (yellow), and schematic extrapolation (for details see Supplemental Material [41]) to large supercells (red). The black arrow indicates a suppression near the band edges (see text).

collection of multiple primitive cells. Accordingly, only a subgroup $\Gamma^{(2)}$ of translations $\Gamma^{(1)}$ is required to generate the lattice. An example pair of primitive cell and supercell of the (Euclidean) $\{4,4\}$ lattice and the (hyperbolic) $\{8,8\}$ lattice is illustrated in Figs. 1(a) and 1(b), respectively.

Dividing the lattice into copies of a chosen cell facilitates PBC, where the lattice is compactified on a closed manifold by identifying sides related by certain translations. On Euclidean lattices, such PBC clusters provide an approximation of the infinite lattice with well-converging bulk properties [46]. To implement PBC on a single cell, opposite sides are identified and the cell is compactified on a torus—independent of its size [Fig. 1(c)]. In contrast, due to the negative curvature, hyperbolic PBC clusters are compactified on manifolds of genus $\mathfrak{g} \geq 2$ [47]. According to the Riemann-Hurwitz formula [48], the genus $\mathfrak{g}_{sc}$ of a compactified supercell grows linearly with the number N of primitive cells:

$$\mathfrak{g}_{sc} - 1 = N(\mathfrak{g}_{pc} - 1), \qquad (1)$$

where $\mathfrak{g}_{pc}$ is the genus of the compactified primitive cell. For the $\{8,8\}$ lattice, the primitive cell is compactified

on a genus-2 surface, and the two-unit-cell supercell (2-supercell) on a genus-3 surface [Fig. 1(d)].

Translation symmetry further enables a reciprocal-space description of the infinite lattice, considering not just a single PBC cluster but also all of its translation-related copies. The choice of cell affects the reciprocal-space description. To illustrate this, consider nearest-neighbor (NN) hopping models on the $\{4,4\}$ and $\{8,8\}$ lattices with Hamiltonian $\mathcal{H} = -\sum_{\langle i,j \rangle} c_i^\dagger c_j$, where $\langle i,j \rangle$ denotes NNs. For Euclidean lattices, the Brillouin zone (BZ) is reduced due to the enlargement of the cell, leading to band folding [Fig. 1(e), inset]; nevertheless, the computed DOS is independent of the cell size. By contrast, in the hyperbolic case, the density of Abelian Bloch states changes significantly when going from a primitive cell to a 2-supercell [Fig. 1(f)]. However, below and in the Supplemental Material [41], we demonstrate that the DOS converges with increasing supercell size.

Real-space perspective.—The symmetries of a $\{p,q\}$ lattice are captured [28,49] by the triangle group Δ generated by reflections a, b, c across the sides of a triangle, called Schwarz triangle, with internal angles $(2\pi/r)$ (with $r = 2$), $(2\pi/q)$, and $(2\pi/p)$ [Figs. 2(b) and 2(c)]. This is reflected in its presentation

$$\Delta(r,q,p) = \langle a,b,c | a^2, b^2, c^2, (ab)^r, (bc)^q, (ca)^p \rangle \qquad (2)$$

with the relators, appearing to the right of the vertical line, set to the identity. Under the action of Δ, copies of the fundamental Schwarz triangle s_f tile the whole plane [see Figs. 2(a) and 2(c) for the $\{8,8\}$ and $\{4,4\}$ lattices, respectively]. Formally, the abstract set S of all
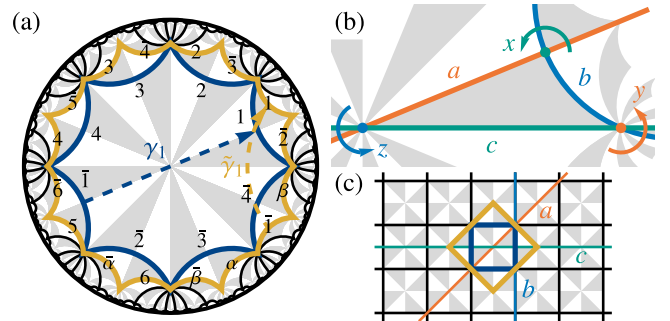
FIG. 2. Symmetries of hyperbolic lattices. (a) $\{8,8\}$ lattice (black lines) with the triangle group $\Delta(2,8,8)$ as space group (indicated by gray/white triangles). The primitive cell (blue polygon) and 2-supercell (yellow polygon) and their edge identifications are shown: the edge $\bar{1}$ is related to 1 by the translation generator γ_1 ($\tilde{\gamma}_1$ for the supercell). Edges related by composite translations are labeled by α and β [41]. (b) Fundamental Schwarz triangle (gray) with reflections a, b, c across the edges of the triangle and rotations $x = ab$, $y = bc$, $z = ca$ around the vertices. (c) Square lattice with primitive cell, supercell, triangle group $\Delta(2,4,4)$, and reflection lines a, b, c.

Schwarz triangles is the orbit of s_f under right action of Δ: $S = s_f \cdot \Delta$.

Interpreted as a space group, Δ encompasses point-group operations and translations. While the point group is generally not a subgroup of Δ (even in Euclidean lattices), translations form a normal subgroup $\Gamma \lhd \Delta$ [50], i.e., any translation conjugated by a reflection or rotation is again a translation. Indeed, Γ is usually defined [12,28] as the largest torsion-free normal subgroup of orientation-preserving elements of Δ, where torsion-freeness captures the absence of elements of finite order in translation groups. Since $\Gamma \lhd \Delta$, the quotient Δ/Γ forms a group and plays the role of the point group. The transversal $T_\Delta(\Gamma)$ is a specific set of representatives of Δ/Γ.

The choice of Γ defines the cell, which comprises a finite number of Schwarz triangles [Fig. 2(a)] and therefore corresponds to a subset $C \subset S$ such that (i) none of the elements are related by translations, and (ii) the right action of Γ on C recovers S, i.e., $S = C \cdot \Gamma$. The coset decomposition $\Delta = \cup_{t \in T_\Delta(\Gamma)} \Gamma t$ implies that $C = s_f \cdot T_\Delta(\Gamma)$. Different choices of $T_\Delta(\Gamma)$ lead to cells C differing in connectedness and symmetry. Our algorithms [39] take Δ/Γ as input, construct random and (for sufficiently small quotients) connected symmetric cells, and extract boundary identifications.

Our supercell method is a natural and systematic way to form sequences of PBC clusters suited to a reciprocal-space interpretation. We construct increasingly larger supercells, by recursively accreting smaller (super)cells in a symmetric fashion, starting with a single primitive cell. This results in a nested sequence of finite-index normal subgroups,

$$\Gamma^{(1)} \rhd \Gamma^{(2)} \rhd \cdots \rhd \Gamma^{(m)} \rhd \cdots, \qquad (3)$$

where $\Gamma^{(m)} \lhd \Delta$ for all m implies normality of the subgroup relationships in Eq. (3). Although there is a unique plane-filling hyperbolic $\{p, q\}$ lattice, the PBC clusters can have different infinite-size limits [27], indicating the choice of sequence is crucial. Recently, Lux and Prodan [34,35] proposed a similar condition with the additional constraint $\cap_{m \geq 1}^{\infty} \Gamma^{(m)} = \{1\}$ and argued that such sequences lead to a well-defined thermodynamic limit [51]. Based on our results, we conjecture that the supercell sequences can be extended in a way that satisfies that additional constraint. While the supercell method does not give a unique sequence, we anticipate that all valid sequences converge to the same limit, consistent with our observations [41].

Translation symmetry allows us to define hopping models by specifying only the hopping amplitudes $h^{uv}(\gamma)$ from site v in the primitive cell $C^{(1)}$ to site u in the primitive cell translated by $\gamma \in \Gamma^{(1)}$. (Here $C^{(m)}$ is the cell associated with the translation group $\Gamma^{(m)}$, and $N^{(m)} = |\Gamma^{(1)}/\Gamma^{(m)}|$ counts primitive cells in $C^{(m)}$.) We additionally subdivide the lattice into copies of the $N^{(m)}$-supercell $C^{(m)}$,

so that the $N^{(m)}$ copies of $C^{(1)}$ in $C^{(m)}$ are generated by the quotient group $\Gamma^{(1)}/\Gamma^{(m)}$. By the coset decomposition, copies of the primitive cell are specified by $\eta_i \tilde{\gamma}$ with transversal elements $\eta_i \in T_{\Gamma^{(1)}}(\Gamma^{(m)})$ and $\tilde{\gamma} \in \Gamma^{(m)}$, and the most general translation-invariant hopping model takes the form [41]

$$\mathcal{H} = \sum_{\substack{\tilde{\gamma}, \tilde{\gamma}' \in \Gamma^{(m)} \\ \eta_i, \eta_j \in T_{\Gamma^{(1)}}(\Gamma^{(m)})}} \sum_{u,v} h^{uv}(\eta_i \tilde{\gamma} \tilde{\gamma}'^{-1} \eta_j^{-1}) c_{\eta_i \tilde{\gamma}}^{u\dagger} c_{\eta_j \tilde{\gamma}'}^{v}, \quad (4)$$

where $\eta_i \tilde{\gamma} \tilde{\gamma}'^{-1} \eta_j^{-1}$ translates the primitive cell at $\eta_j \tilde{\gamma}'$ to that at $\eta_i \tilde{\gamma}$. Our algorithms [39,52] define hopping models on unit cells and extend models defined on a primitive cell to a supercell according to Eq. (4).

Reciprocal-space perspective.—In Euclidean lattices, translation symmetry constrains the form of Hamiltonian eigenstates via Bloch's theorem [53]. Similarly, the automorphic Bloch theorem for hyperbolic lattices [27] stipulates that eigenstates ψ_D of a translation-invariant Hamiltonian satisfy $\psi_D[\gamma^{-1}(z)] = D(\gamma)\psi_D(z)$, where $\gamma \in \Gamma$ is a translation, z the position coordinate, and D an IR of Γ. By contrast with Euclidean lattices, Γ has IRs of dimensions $d > 1$. Nevertheless, we can block-diagonalize [41] the Hamiltonian in Eq. (4) into blocks of Bloch Hamiltonians,

$$H(D) = \sum_{\tilde{\gamma} \in \Gamma^{(m)}} \mathsf{h}(\tilde{\gamma}) \otimes D(\tilde{\gamma}), \qquad (5)$$

where $\mathsf{h}_{ij}^{uv}(\tilde{\gamma}) = h^{uv}(\eta_i \tilde{\gamma} \eta_j^{-1})$ is the hopping matrix within the supercell, and the unitary $(d \times d)$-matrix $D(\tilde{\gamma})$ generalizes the Bloch phase factor [14].

Generally, no parametrization of the IRs D is known, limiting a direct application of the automorphic Bloch theorem. However, the space of 1D IRs, the Abelian BZ (ABZ), is well understood: if the cell is compactified on a manifold of genus $\mathfrak{g}$, then ABZ is the $2\mathfrak{g}$-dimensional torus $\mathsf{T}^{2\mathfrak{g}}$ parametrized by momenta $\{0 \leq k_i < 2\pi\}_{i=1}^{2\mathfrak{g}}$ and the IRs are defined on the $2\mathfrak{g}$ generators γ_i of Γ by $D_{\mathbf{k}}(\gamma_i) = e^{ik_i}$ [26–28]. While the ABZ sometimes is representative of the bulk spectrum of flakes [10–12,23], important features can be missed [36,37]. Studying the non-Abelian Bloch states is therefore crucial for a complete reciprocal-space description. Remarkably, as we explain below, AHBT applied to a sequence of supercells provides systematic access to non-Abelian Bloch states.

Considering the sequence of translation groups in Eq. (3), each $\Gamma^{(m)}$ has a tower of d-dimensional IRs with $d \geq 1$ (Fig. 3). However, due to the subgroup relationships, the IRs of different $\Gamma^{(m)}$ are *not* independent. First, the restriction of a d-dimensional IR of $\Gamma^{(m)}$ to its subgroup $\Gamma^{(m+1)}$ is a d-dimensional (possibly reducible) *subduced* representation of $\Gamma^{(m+1)}$. Second, any d-dimensional IR of
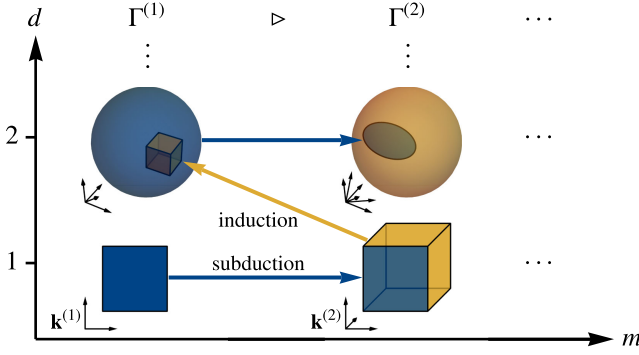
FIG. 3. Illustration of the spaces of d-dimensional irreducible representations (IRs) of a sequence of translation subgroups $\Gamma^{(m)}$ corresponding to supercells with $N^{(m)}$ primitive cells. The spaces of 1D IRs are hypertori (illustrated as square and cube) with dimension growing linearly with $N^{(m)}$, while the spaces of higher-dimensional IRs are more complicated (illustrated as balls). The IRs of $\Gamma^{(m)}$ of dimension d subduce (blue arrow) representations of $\Gamma^{(m+1)}$ of the same dimension and induce (yellow arrow) representations of $\Gamma^{(m-1)}$ of higher dimension (see text).

$\Gamma^{(m)}$ implies a $(d|\Gamma^{(m-1)}/\Gamma^{(m)}|)$-dimensional (possibly reducible) *induced* representation of $\Gamma^{(m-1)}$ [54]. Thus, 1D IRs of $\Gamma^{(m)}$ subduce 1D IRs of $\Gamma^{(m+1)}$, but because $\mathrm{ABZ}^{(m+1)}$ has larger dimension than $\mathrm{ABZ}^{(m)}$, there must be 1D IRs of $\Gamma^{(m+1)}$ that induce higher-dimensional IRs of $\Gamma^{(m)}$. Therefore, by studying the well-understood 1D IRs of supercells in the sequence, we gain access to a successively larger portion of higher-dimensional IRs of $\Gamma^{(1)}$. While this scheme does not reproduce *all* IRs, we conjecture that it converges to the thermodynamic limit [35] for $m \to \infty$.

Results.—We illustrate the supercell method by computing the DOS for selected hopping models on hyperbolic lattices: the previously studied octagon-kagome [11] and $\{8,3\}$-Haldane [10,12] models, and a generalization to the $\{6,4\}$ lattice of the Benalcazar-Bernevig-Hughes (BBH) model [55]. Each model is defined on a symmetric primitive cell and the DOS is computed [41] by randomly sampling $\mathrm{ABZ}^{(m)}$ in a sequence satisfying Eq. (3). We observe rapid convergence with system size: Figs. 4(a), 4(b), and 5(b) show data for systems with only up to 32 (768), 32 (512), and 64 (1536) primitive cells (sites), respectively. In sharp contrast, the DOS obtained from the corresponding PBC cluster (without applying AHBT) is extremely far from converged [41], demonstrating the computational power of our approach.

The NN hopping model on the octagon-kagome lattice has been analyzed in the context of flat bands in Ref. [11]. Using real-space arguments, the authors describe a band touching between the flat band and the dispersive bands. In Fig. 4(a), we observe that the DOS near the flat band is suppressed with increasing number of primitive cells N, suggesting that the gaplessness is a
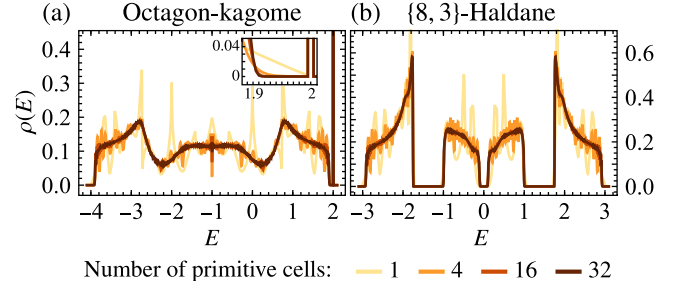
FIG. 4. Density of states $\rho(E)$ as function of energy E of (a) the nearest-neighbor (NN) model on the octagon-kagome lattice and (b) the Haldane model on the $\{8,3\}$ lattice with NN hopping $h_1 = 1$, next-NN hopping $h_2 = 1/6$, flux $\phi = \pi/2$, and sublattice mass $h_0 = 1/3$. The inset in (a) shows the depletion of $\rho(E)$ near the flat band at $E = 2$.

finite-size effect. This DOS suppression is consistent with the expected behavior near a band edge. Assuming a generic quadratic scaling of the energy dispersion with (Abelian) momentum near the band touching, $E \propto \mathbf{k}^2$, we obtain the DOS by integrating over the $2\mathfrak{g}$-dimensional ABZ: $\rho(E) \sim \int \mathrm{d}^{2\mathfrak{g}}\mathbf{k}\,\delta(E - v\mathbf{k}^2) \propto E^{\mathfrak{g}-1}$. Since $\mathfrak{g}$ grows linearly with N [Eq. (1)], this explains the DOS suppression near band edges, indicated in Fig. 1(f) and observed in all models [Figs. 4 and 5(b)].

Next, we turn to the Haldane model on the $\{8,3\}$ lattice [10,12] which generalizes the original Haldane model on the honeycomb lattice [56]. We adopt the parameter choices of Ref. [10] and show the converging DOS in Fig. 4(b). Crucially, the characteristic DOS suppression near the edges of all three gaps indicates that the gaps obtained from AHBT are stable to the inclusion of non-Abelian Bloch states and are not caused by finite-size effects.
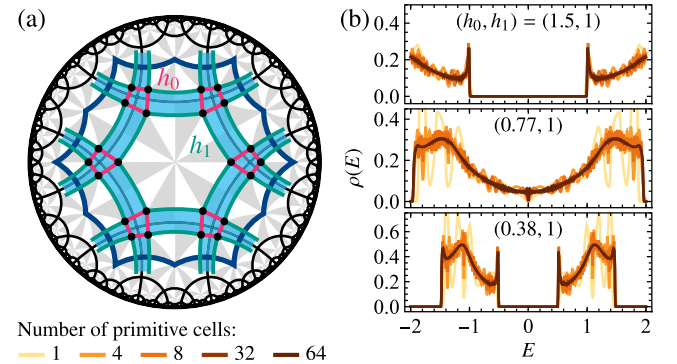
FIG. 5. Benalcazar-Bernevig-Hughes model on the $\{6,4\}$ lattice. (a) Model definition on the primitive cell (blue polygon) of the $\{6,4\}$ lattice (black lines). There are four orbitals (black dots) at each site, coupled by intersite hoppings h_0 (magenta) and intrasite hoppings h_1 (green). Light blue shading of plaquettes bounded by magenta and green lines indicates π fluxes. (b) Density of states for the indicated choices of (h_0, h_1). The top, middle, and bottom subpanels correspond to the trivial, critical, and nontrivial phases, respectively.

Finally, motivated by the recent interest in higher-order topological phenomena on hyperbolic flakes [16,17], we introduce the BBH model on the $\{6, 4\}$ lattice. Similar to its original version on the square lattice [55], the model is defined on a lattice with fourfold coordination, has four orbitals per site, and exhibits π fluxes through the quadrilateral plaquettes [Fig. 5(a)]. The intrasite hopping h_0 may differ from the intersite hopping h_1. As in the Euclidean case, this arrangement leads to a *trivial* phase for $|h_0| \gg |h_1|$ with effectively independent rings centered at lattice sites, and a *nontrivial* phase for $|h_0| \ll |h_1|$ with effectively independent rings centered on the plaquettes. The computed DOS for the two phases and the transition are shown in Fig. 5(b). The trivial and the nontrivial phases both exhibit an energy gap that remains stable when going to larger supercells. The gap closes at $h_0/h_1 \approx 0.77$, indicating a phase transition. Interestingly, for small supercells the transition appears semimetallic with vanishing DOS at $E = 0$. However, this is a finize-size effect and the DOS ultimately converges to a finite value, implying a metallic transition.

Conclusions.—We have introduced a method for systematically studying non-Abelian Bloch states in hyperbolic lattices by applying Abelian hyperbolic band theory to sequences of supercells, in analogy to zone folding in solid-state physics. This provides a substantial step toward a complete reciprocal-space description, which we believe to be consistent with recent work [34,35] in real space. While real-space methods scale suboptimally due to the increasing number of noncontractible loops [37], the combination of real-space supercells with reciprocal-space momenta in our approach appears to mitigate this problem and additionally provides true bulk states instead of finite-size approximations. Our DOS results on gapless elementary nearest-neighbor models are in agreement with previous results obtained using a different method [37], but we additionally studied topological models exhibiting energy gaps. Our method has three substantial advantages over Ref. [37]: (i) it gives direct access to bulk eigenstates, (ii) it allows for parallel computation through separating the Hilbert space into **k** sectors, and (iii) there is no extra computational cost for longer-range hoppings.

Looking ahead, we anticipate our reciprocal-space supercell method will facilitate advances in HBT such as symmetry analysis [12], low-energy expansions [36], and topological band theory, including the recently studied 2D hyperbolic model [22] with nontrivial second Chern number [36]. Developing systematic algorithms for generating longer sequences of $\Delta/\Gamma^{(m)}$ quotients beyond those in Ref. [38] would be beneficial for achieving better convergence. Finally, we hope the implementation of our approach in a publicly available software package [39,52,57] will accelerate further studies of hyperbolic quantum matter.

[*] plengg@pks.mpg.de
[†] maciejko@ualberta.ca
[‡] tomas.bzdusek@uzh.ch

[1] A. J. Kollár, M. Fitzpatrick, and A. A. Houck, Hyperbolic lattices in circuit quantum electrodynamics, Nature (London) **571**, 45 (2019).

[2] P. M. Lenggenhager, A. Stegmaier, L. K. Upreti, T. Hofmann, T. Helbig, A. Vollhardt, M. Greiter, C. H. Lee, S. Imhof, H. Brand, T. Kießling, I. Boettcher, T. Neupert, R. Thomale, and T. Bzdušek, Simulating hyperbolic space on a circuit board, Nat. Commun. **13**, 4373 (2022).

[3] S. Yu, X. Piao, and N. Park, Topological hyperbolic lattices, Phys. Rev. Lett. **125**, 053901 (2020).

[4] I. Boettcher, P. Bienias, R. Belyansky, A. J. Kollár, and A. V. Gorshkov, Quantum simulation of hyperbolic space with circuit quantum electrodynamics: From graphs to geometry, Phys. Rev. A **102**, 032208 (2020).

[5] A. Saa, E. Miranda, and F. Rouxinol, Higher-dimensional Euclidean and non-Euclidean structures in planar circuit quantum electrodynamics, arXiv:2108.08854.

[6] X. Zhu, J. Guo, N. P. Breuckmann, H. Guo, and S. Feng, Quantum phase transitions of interacting bosons on hyperbolic lattices, J. Phys. Condens. Matter **33**, 335602 (2021).

[7] A. Stegmaier, L. K. Upreti, R. Thomale, and I. Boettcher, Universality of Hofstadter butterflies on hyperbolic lattices, Phys. Rev. Lett. **128**, 166402 (2022).

[8] M. Ruzzene, E. Prodan, and C. Prodan, Dynamics of elastic hyperbolic lattices, Extreme Mech. Lett. **49**, 101491 (2021).

[9] P. Bienias, I. Boettcher, R. Belyansky, A. J. Kollár, and A. V. Gorshkov, Circuit quantum electrodynamics in hyperbolic space: From photon bound states to frustrated spin models, Phys. Rev. Lett. **128**, 013601 (2022).

[10] D. M. Urwyler, P. M. Lenggenhager, I. Boettcher, R. Thomale, T. Neupert, and T. Bzdušek, Hyperbolic topological band insulators, Phys. Rev. Lett. **129**, 246402 (2022).

[11] T. Bzdušek and J. Maciejko, Flat bands and band-touching from real-space topology in hyperbolic lattices, Phys. Rev. B **106**, 155146 (2022).

[12] A. Chen, Y. Guan, P. M. Lenggenhager, J. Maciejko, I. Boettcher, and T. Bzdušek, Symmetry and topology of hyperbolic Haldane models, Phys. Rev. B **108**, 085114 (2023).

[13] R. Mosseri, R. Vogeler, and J. Vidal, Aharonov-Bohm cages, flat bands, and gap labeling in hyperbolic tilings, Phys. Rev. B **106**, 155120 (2022).

[14] N. Cheng, F. Serafin, J. McInerney, Z. Rocklin, K. Sun, and X. Mao, Band theory and boundary modes of high-dimensional representations of infinite hyperbolic lattices, Phys. Rev. Lett. **129**, 088002 (2022).

[15] Z.-R. Liu, C.-B. Hua, T. Peng, and B. Zhou, Chern insulator in a hyperbolic lattice, Phys. Rev. B **105**, 245301 (2022).

[16] Y.-L. Tao and Y. Xu, Higher-order topological hyperbolic lattices, Phys. Rev. B **107**, 184201 (2023).

[17] Z.-R. Liu, C.-B. Hua, T. Peng, R. Chen, and B. Zhou, Higher-order topological insulators in hyperbolic lattices, Phys. Rev. B **107**, 125302 (2023).

[18] P. Basteiro, G. D. Giulio, J. Erdmenger, J. Karl, R. Meyer, and Z.-Y. Xian, Towards explicit discrete holography: Aperiodic spin chains from hyperbolic tilings, SciPost Phys. **13**, 103 (2022).

[19] P. Basteiro, R. N. Das, G. D. Giulio, and J. Erdmenger, Aperiodic spin chains at the boundary of hyperbolic tilings, arXiv:2212.11292.

[20] N. Gluscevich, A. Samanta, S. Manna, and B. Roy, Dynamic mass generation on two-dimensional electronic hyperbolic lattices, arXiv:2302.04864.

[21] W. Zhang, H. Yuan, N. Sun, H. Sun, and X. Zhang, Observation of novel topological states in hyperbolic lattices, Nat. Commun. **13**, 2937 (2022).

[22] W. Zhang, F. Di, X. Zheng, H. Sun, and X. Zhang, Hyperbolic band topology with non-trivial second Chern numbers, Nat. Commun. **14**, 1083 (2023).

[23] A. Chen, H. Brand, T. Helbig, T. Hofmann, S. Imhof, A. Fritzsche, T. Kießling, A. Stegmaier, L. K. Upreti, T. Neupert, T. Bzdušek, M. Greiter, R. Thomale, and I. Boettcher, Hyperbolic matter in electrical circuits with tunable complex phases, Nat. Commun. **14**, 622 (2023).

[24] Q. Pei, H. Yuan, W. Zhang, and X. Zhang, Engineering boundary-dominated topological states in defective hyperbolic lattices, Phys. Rev. B **107**, 165145 (2023).

[25] J. Chen, F. Chen, Y. Yang, L. Yang, Z. Chen, Y. Meng, B. Yan, X. Xi, Z. Zhu, G.-G. Liu, P. P. Shum, H. Chen, R.-G. Cai, R.-Q. Yang, Y. Yang, and Z. Gao, AdS/CFT correspondence in hyperbolic lattices, arXiv:2305.04862.

[26] J. Maciejko and S. Rayan, Hyperbolic band theory, Sci. Adv. **7**, abe9170 (2021).

[27] J. Maciejko and S. Rayan, Automorphic Bloch theorems for hyperbolic lattices, Proc. Natl. Acad. Sci. U.S.A. **119**, e2116869119 (2022).

[28] I. Boettcher, A. V. Gorshkov, A. J. Kollár, J. Maciejko, S. Rayan, and R. Thomale, Crystallography of hyperbolic lattices, Phys. Rev. B **105**, 125118 (2022).

[29] K. Ikeda, S. Aoki, and Y. Matsuki, Hyperbolic band theory under magnetic field and Dirac cones on a higher genus surface, J. Phys. Condens. Matter **33**, 485602 (2021).

[30] K. Ikeda, Y. Matsuki, and S. Aoki, Algebra of hyperbolic band theory under magnetic field, arXiv:2107.10586.

[31] E. Kienzle and S. Rayan, Hyperbolic band theory through Higgs bundles, Adv. Math. **409**, 108664 (2022).

[32] Á. Nagy and S. Rayan, On the hyperbolic Bloch transform, Ann. Henri Poincaré (2023), 10.1007/s00023-023-01336-8.

[33] A. Attar and I. Boettcher, Selberg trace formula in hyperbolic band theory, Phys. Rev. E **106**, 034114 (2022).

[34] F. R. Lux and E. Prodan, Spectral and combinatorial aspects of Cayley-crystals, Ann. Henri Poincaré. (2023).

[35] F. R. Lux and E. Prodan, Converging periodic boundary conditions and detection of topological gaps on regular hyperbolic tessellations, Phys. Rev. Lett. **131**, 176603 (2023).

[36] T. Tummuru, A. Chen, P. M. Lenggenhager, T. Neupert, J. Maciejko, and T. Bzdušek, Hyperbolic non-Abelian semimetal, arXiv:2307.09876.

[37] R. Mosseri and J. Vidal, Density of states of tight-binding models in the hyperbolic plane, Phys. Rev. B **108**, 035154 (2023).

[38] M. Conder, Quotients of triangle groups acting on surfaces of genus 2 to 101 (2007), https://www.math.auckland.ac.nz/~conder/TriangleGroupQuotients101.txt.

[39] P. M. Lenggenhager, J. Maciejko, and T. Bzdušek, HYPER-CELLS package for GAP (2023), https://github.com/patrick-lenggenhager/HyperCells.

[40] GAP, GAP—Groups, Algorithms, and Programming, Version 4.11.1, The GAP Group (2021).

[41] See Supplemental Material at http://link.aps.org/supplemental/10.1103/PhysRevLett.131.226401, which cites additional Ref. [42–45], for further information on the definition of hopping models, the derivation of the Bloch Hamiltonian, the convergence of the supercell method, and on the models and data presented here.

[42] J. Cano and B. Bradlyn, Band representations and topological quantum chemistry, Annu. Rev. Condens. Matter Phys. **12**, 225 (2020).

[43] A. E. Brouwer and W. H. Haemers, *Spectra of Graphs* (Springer, New York, 2012).

[44] D. J. S. Robinson, *A Course in the Theory of Groups*, 2nd ed. (Springer, New York, 1996).

[45] T. Bzdušek and M. Sigrist, Robust doubly charged nodal lines and nodal surfaces in centrosymmetric systems, Phys. Rev. B **96**, 155105 (2017).

[46] N. W. Ashcroft and N. D. Mermin, *Solid State Physics* (Holt-Saunders, 1976).

[47] F. Sausset and G. Tarjus, Periodic boundary conditions on the pseudosphere, J. Phys. A **40**, 12873 (2007).

[48] R. Miranda, *Algebraic Curves and Riemann Surfaces* (American Mathematical Society, Providence, 1995).

[49] W. Magnus, *Noneuclidean Tesselations and Their Groups* (Academic Press, New York, 1974).

[50] C. J. Bradley and A. P. Cracknell, *The Mathematical Theory of Symmetry in Solids: Representation Theory for Point Groups and Space Groups* (Clarendon Press, Oxford, 1972).

[51] W. Lück, Approximating L^2-invariants by their finite-dimensional analogues, Geom. Funct. Anal. **4**, 455 (1994).

[52] P. M. Lenggenhager, J. Maciejko, and T. Bzdušek, HYPERBLOCH package for Mathematica (2023), https://github.com/patrick-lenggenhager/HyperBloch.

[53] F. Bloch, Über die Quantenmechanik der Elektronen in Kristallgittern, Z. Phys. **52**, 555 (1929).

[54] W. Fulton and J. Harris, *Representation Theory* (Springer, New York, 1991).

[55] W. A. Benalcazar, B. A. Bernevig, and T. L. Hughes, Quantized electric multipole insulators, Science **357**, 61 (2017).

[56] F. D. M. Haldane, Model for a quantum Hall effect without Landau levels: Condensed-matter realization of the "parity anomaly", Phys. Rev. Lett. **61**, 2015 (1988).

[57] P. M. Lenggenhager, J. Maciejko, and T. Bzdušek, Supplementary data and code for: Non-Abelian Hyperbolic Band Theory from Supercells (2023), 10.5281/zenodo.10142168.